Peremennye Zvezdy (*Variable Stars*) **31**, No. 5, 2011

Received October 1; accepted October 17.

Photometric Mass Estimate for the Compact Component of SS 433: And Yet It Is a Neutron Star

V. P. Goranskij

Sternberg Astronomical Institute, M.V. Lomonosov Moscow University, Universitetski pr., 13, Moscow, 199992, Russia;
e-mail: goray@sai.msu.ru

After 33 years of extensive studies of SS 433, we have learnt much about this unique system with moving emission lines in the spectrum. The orbital inclination is known from spectroscopic observations of moving lines; the distance is derived from radio interferometry of relativistic jets; the mass ratio of its components is determined from X-ray observations of jets' eclipses. In 2005, the accretion donor was detected as an A4–A8 giant, and its contribution to eclipse light was measured spectroscopically. In the present paper, the A-type star was detected via multicolor photometry on the basis of its Balmer jump. A method is proposed to estimate the interstellar reddening, able to measure the individual law of interstellar absorption for SS 433 from spectrophotometry. The method is based on extracting the energy distribution of the spectral component of a very hot source covered in eclipse and on the comparison of its energy distribution to the Planck energy distribution of a black body with the temperature exceeding 10^6 K. The determination of general parameters of SS 433 leads to fairly accurate estimates of luminosity, radius, and mass of the A star in the system, and consequently leads to an accurate estimate of the mass of the compact component, the source of jets. The latter mass is between 1.25 and 1.87 solar masses. The reasons for overestimating this mass when using the dynamical method are discussed. In our opinion, the presence of a black hole in this system is excluded.

1 INTRODUCTION

SS 433 (Stephenson & Sanduleak, 1977) = V1343 Aql is a unique variable star with moving emission lines in the spectrum. Each stationary emission of Balmer or HeI lines has two moving emission components that are formed by a pair of oppositely directed and highly collimated precessing relativistic jets or beams of very hot matter accelerated to the velocity of $0.26c$, i.e. to ~ 80000 km/s. The period of jet precession is $162\overset{\mathrm{d}}{.}5$–$164^{\mathrm{d}}$ (Margon et al., 1979; Margon, 1984). The jets are inclined to the precession axis by $19\overset{\circ}{.}75$, and the axis of precession is inclined by $78\overset{\circ}{.}81$ to the line of sight (Davydov et al., 2008). Like wavelengths of other moving lines, the wavelengths of H_α components follow sine functions with the full amplitudes of 1200 Å, in antiphase (Fig. 1). In this motion, H_α components are superimposed in the position located near 6800 Å twice for a precession period, at the times usually designated T_1 and T_2. The wavelength where the components coincide differs from the stationary H_α-line wavelength by 250 Å, and this is due to transverse Doppler effect following from the special theory of relativity. The time of the largest divergence of moving emissions is designated T_3. Additionally, the jets show nodding oscillations (or jitter) with the period of $6\overset{\mathrm{d}}{.}28$ (Newsom & Collins, 1981 and 1986; Wagner et al., 1981) and amplitude of $2\overset{\circ}{.}8$ (Borisov & Fabrika, 1987). The matter of jets is erupted into "bullets" that become apparent as discrete line components in the spectra, so that each emission detail appears at a fixed wavelength, it strengthens in a typical time range of about 0.5–1^{d} and decays in 1–3^{d} (Grandi & Stone, 1982; Vermeulen et al., 1993a). Several bullets form the composite structure of a moving emission line. The collimation angle of a bullet is about $1\overset{\circ}{.}0$–$1\overset{\circ}{.}4$ (Borisov & Fabrika, 1987).

The details of precessing jets can be followed by radio interferometry in the milliarcsecond scale (Vermeulen et al., 1993b). Deep radio images were taken with the VLA radio telescope, they show the structure of jets up to angular distances of 4″(Blundell & Bowler, 2004). Fitting radio images with the kinematical model of jets gives a sufficiently accurate distance to SS 433, independent of interstellar absorption. This distance is in the range between 4.85 (Vermeulen et al., 1993b, from the VLBI) and 5.50 kpc (Hjellming & Johnson, 1982, from the VLA, and Blundell & Bowler, 2004, from the VLA). Intermediate distance values were measured with the same method by Spencer (1984), MERILIN, 4.9 kpc; Fejes (1986), VLBI, 5.0 kpc; and Romney et al. (1987), VLBI, 5.0 kpc. There is no systematical trend of distance measures versus time, and the mean distance value is 5.12 ± 0.27 kpc.

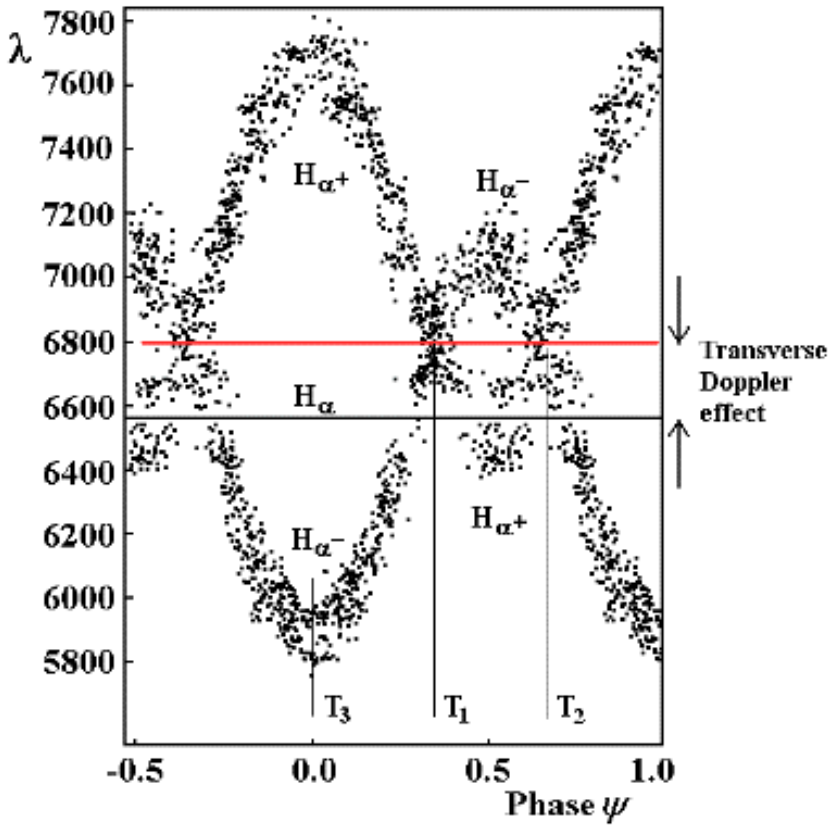

Figure 1. Wavelengths of the H_α^+ and H_α^- moving components versus precession phase ψ. The black horizontal line marks the location of the stationary H_α emission line. The red horizontal line is the axis of symmetry passing through the points of coincidence of the moving components T_1 and T_2. The zero point of precession phase is adopted at T_3.

SS 433 is also known as an eclipsing binary system with the orbital period of $13\overset{\text{d}}{.}082$ (Gladyshev et al., 1980; Gladyshev, 1981; Cherepashchuk, 1981; Crampton & Hutchings, 1981). In kinematical jet-precession models derived from observations of the moving lines, the axis of precession coincides with the orbital axis, so the orbital inclination of SS 433 is measured correctly. Photometry of SS 433 also reveals precession and nodding periods, as well as light outbursts at different time scales (Goranskii et al., 1998a). The shape of eclipsing light curve and its maximum light depend on the phase of precession period (Fig. 2). Near T_3 times, it looks like that of a typical β Lyrae variable star having two minima of different depths. At other phases of precession, the dispersion of observations

increases, but some orbital-phase averaged light curves resemble those of Cepheids. There are pronounced brightness variations in eclipse depth depending on the precession-period phase ψ, with the V-band amplitude of $0\overset{\mathrm{m}}{.}4$. These variations suggest that the eclipses are partial. However, the same variations can be fitted by the nodding period as well because the precession and nodding periods are related to the orbital one by the formula:

$$1/P_{nod} = 2/P_{orb} + 1/P_{prec}, \tag{1}$$

and thus, phases of nodding and precession periods are similar if the observations are chosen from a narrow range of the orbital phase (during the eclipse). This means that we cannot distinguish precessing and nodding light variations in the eclipse depth.

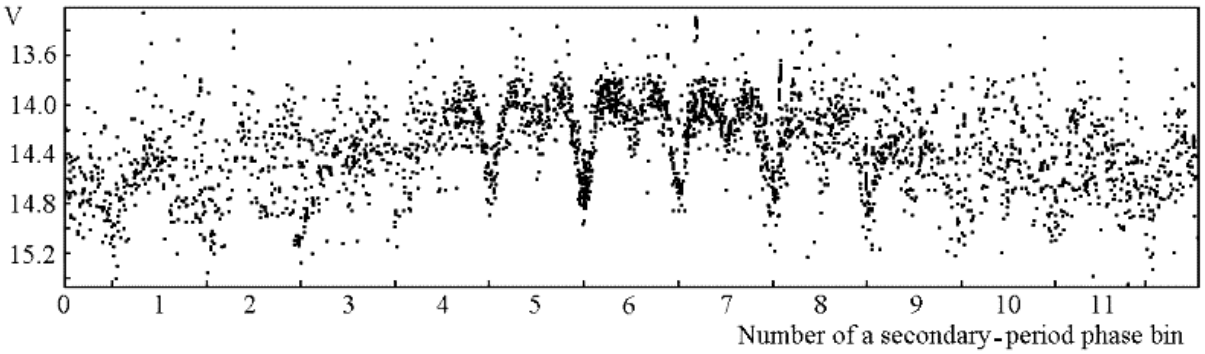

Figure 2. Evolution of the orbital light curve with the phase of the secondary precession period. To demonstrate the effect, the orbital-period light curves are calculated in 12 intervals (bins) of the precession period and displayed in the order of increasing precession phase. The precession zero phase T_3 corresponds to the bin No. 6. Several observations are out of this magnitude range and are not plotted.

Multicolor photometry reveals peculiar behavior of SS 433 in different filters. If the $U-B$ and $B-V$ color indices remain approximately constant and independent of brightness, the $V-R$ index varies with the orbital phase, being strongly correlated with the V or R magnitudes. During flares or active states, the $V-R$ index departs from this relation to the right side (Gladyshev, 1981), suggesting that the deviations are connected with a brightening of the stationary H_α emission. However, observations in the $UBVRI(\mathrm{H}_\alpha)$ filters in a flare performed by V. Rakhimov (Aslanov et al., 1993) revealed that the amplitude of the flare in the near-infrared I filter (λ_{eff} = 7700 Å; FWHM = 1040 Å) was larger than in the narrow-band H_α filter (λ_{eff} = 6550 Å; FWHM = 200 Å). This phenomenon was noticed by an anonymous referee of the *Astronomy and Astrophysics*, so we call it "the anonymous referee effect". The referee's finding led to a chain of further discoveries. First, it was found that the light curve of SS 433 consisted of two almost independent light curves formed by two light sources having essentially different $V-R$ color indices, $1\overset{\mathrm{m}}{.}9$ and $2\overset{\mathrm{m}}{.}8$. Second, both light curves may be easily extracted from the combined light curve. Third, the blue source shows periodic orbital, precessing, and nodding variations, whereas the red one is not periodic and exhibits flares that coincide with radio flares (Goranskij et al., 1998b). It became clear that the spectrum of the red source extended up to radio wavelengths. Its contribution to the combined spectrum of the system increases to longer wavelengths. The red source veils the blue source, and therefore amplitudes of the orbital and precession light variations decrease from U, B, V to J, H, K bands. The contribution of the blue source is variable with the orbital period, and this is a reason why the $V-R$ index varies with the orbital phase.

The mean $U-B$ and $B-V$ colors of SS 433 are respectively $0\overset{\mathrm{m}}{.}90$ and $2\overset{\mathrm{m}}{.}20$. They are strongly subject to interstellar reddening. These indices suggest that SS 433 is a hot OB star with the reddening $E(B-V) \approx 2\overset{\mathrm{m}}{.}53$ and the full extinction A_V of approximately 8^{m} (Murdin et al., 1980; Cherepashchuk et al., 1982; Margon, 1984). Wagner (1986) found $A_V = 7.8^{\mathrm{m}} \pm 0.5^{\mathrm{m}}$ from continuum fitting of spectrophotometric observations in the wavelength range between 4036 and 8100 Å. The mean color temperature was about 32500 K, the continuum spectrum appeared hotter when the precessing body was brighter, and these variations corresponded to an amplitude of $0\overset{\mathrm{m}}{.}08$ in the $B-V$ color.

The most valuable information on jet structure and mass ratio of the components of SS 433 can be derived from X-ray observations of its eclipses. The Ginga X-ray observatory has made the most important contribution to the research of SS 433. Three eclipses were continuously monitored with a complete phase coverage at different phases of the precession period, namely those in May 1987, May 1988 and May 1999; additional pointings to the object were performed at different orbital and precession phases (Yuan et al., 1995). It became clear that most X-rays were emitted from the jets. The shape of the continuum could be fitted with a single thermal bremsstrahlung model, its characteristic temperature kT_0 being about 20 keV. With the eV-to-Kelvin reduction coefficient of $1.1604 \cdot 10^4$, this temperature is $232 \cdot 10^6$ K. Thus, there exists an uncovered source with a temperature that high in the system. Note that one cannot distinguish thermal sources with temperatures above 10^6 K using multicolor $UBVRI$ photometry because their spectral energy distributions (SEDs) have maxima far in the X-rays and their slopes are similar in the $UBVRI$ spectral region. Such energy distributions do not differ much from those of an O-type star with a temperature about 32500 K (Wagner, 1986), and their color temperature can be underestimated due to the contribution from the red and infrared excess, discovered with the help of the referee. Ginga observations also show a strong K emission blend of Fe XXV/Fe XXVI at 6 keV that can be extracted from the spectrum. The line shows the same relativistic shifts as the moving "violet" (short-wavelength) components of the Balmer emission. Some observations made near T_1 and T_2 also display a moving "red" component from the oppositely directed jet.

X-ray eclipses of SS 433 are partial and show strongly pronounced contacts of the jet base with the companion's limb. One of the eclipses registered by Ginga, centered at 1987 May 20.9 ± 0.5 UT (precession phase $\psi = 0.25$ if counted from T_3), occurred in the high state (a strong flux and hard spectrum) (Kawai et al., 1989; Brinkmann et al., 1989). The duration of the eclipse measured as the time interval between contacts is $2\overset{\mathrm{d}}{.}4$. The shape of the eclipse is similar in different energy bands, the intensity of the extracted K_α line shows variations with the same contacts and the same relative depth. This observation confirms that it is the jet that is eclipsed, and the jet is the brightest X-ray source in the system. Additionally, these observations along with the well-known orbital inclination enable us to measure the mass ratio of the components very accurately. With the standard assumption that the optical star fills its Roche lobe and using Paczynski's formula for the size of the Roche lobe,

$$R_*/a = 0.38 - 0.2 \cdot \log_{10}(q) \approx 0.545 \qquad (2)$$

in this case, Brinkmann et al. (1989) obtained the ratio $q = M_x/M_{opt} = 0.1496$. In Paczynski's formula, R_* is the radius of the optical star and a is the binary's separation. Using the results of Doppler analysis of the stationary HeII lines by Crampton and Hutchings (1981), Brinkman et al. (1989) derived the masses $2.1M_\odot$ and $14M_\odot$ for the components and the optical component's radius $32R_\odot$. With such a mass ratio, one should expect that, in eclipses, the donor covers the full Roche-lobe volume of the compact companion, including the surrounding accretion disk if it exists. This simple solution is

based on the assumption that the jet is thin, i.e. its width is negligibly small compared to the radius of the optical star.

Kawai et al. (1989) considered solutions for q based on wider assumptions like opposed jets, a thick accretion disk around the compact object, a thick jet with a cylindrical axisymmetric shape. These assumptions disperse the values of q in the 0.13–4.6 range. Different authors considered a cocoon instead of a jet, or an eclipse of the jet by a star having an extended outflowing envelope without any clear-cut limb. All these attempts were made to increase q. In my opinion, a thin jet is a satisfactory solution. Actually, no additional contacts are seen in the shape of X-ray eclipses that would look like intensity jumps. In the case of a thin jet, the exponential intensity decrease along its length can be revealed from observations, it is described with the following formula:

$$I(x) = a \cdot exp(-1.8x/R_*), \tag{3}$$

where x is the length measured from the base. This formula can be derived with the technique of lost light as follows. First, we interpolate the out-of-eclipse flux to the phase range of the eclipse and measure the flux deficiency due to the eclipse for each in-eclipse observation. Second, we calculate the covered length of the jet for the phase of each point in a simple model. The relation of flux deficiency versus covered length can well be fitted with an exponent function; the points of ingress and egress fall on the same line in spite of the different rate of variation. A steep ingress of this eclipse means that the base of the thin jet is directed along the star limb, and the base disappears rapidly. Contrary, the egress is slow; this means that the jet base reappears from behind the limb at a large angle. This behavior corresponds to precession phase 0.25 for the retrograde motion of the jet with respect of the orbital motion. The relation of intensity versus jet length can be revealed by differentiating the averaged flux deficiency function. Naturally, we would not be able to see such a behavior were the jet thick and were the thickness of the jet covered in ingress or egress. Our model light curves for May 1987 X-ray eclipse were published by Goranskij et al. (1997, Fig. 2), and by Goranskij (1998c, Fig. 2). From this model, with the jet base located in the orbital plane, we found $q = 0.155 \pm 0.015$. This value may be even less if the base of the visible jet is above the plane. This is in a very good agreement with the results from Brinkmann et al. (1989).

ASCA high-resolution X-ray spectral observations performed on April 23 and 24, 1993 resolved the K_α blend at 6 keV into Fe XXV and Fe XXVI lines; each line showed both a strong "violet" component and a faint "red" one (Kotani et al., 1994). Both components had large Doppler shifts, and positions of components in the spectra agreed with the kinematical model. Detections of moving lines of Ar XVII, Ar XVIII, S XV, S XVI, Ca XIX, and Ni XXVII ions were also reported. XMM observations (Brinkmann et al., 2005) also confirm large Doppler-shifted emission components; the "red" jet contributes 30–40 percents to the total photon flux. The best estimates of the temperature at the jet base are around $kT_0 \sim 17 \pm 2$ keV. The "stationary line" in K_α around 7 keV was found in the Ginga data, but not in later ASCA and Chandra observations (Brinkmann et al., 2005). The XMM K_α line profiles seem to be strongly affected by the "stationary line", which may be an indicator of Compton scattering of jet base radiation on surrounding cold matter. One eclipse, dated 2003 May 11, was observed by the INTEGRAL X-ray observatory in hard X-rays ranged between 25 and 100 keV during a large campaign including optical spectroscopy, optical and infrared photometry (Cherepashchuk et al., 2005). Unfortunately, the phase coverage of the eclipse in hard rays was insufficient. Nevertheless, fragments of light curves suggest that the width of the hard X-ray eclipse is larger than in soft X-rays; probably the width increases with energy. The hard X-ray eclipse is at least two times deeper than the soft X-ray eclipse. No contacts were

seen. Thus, the authors treat the eclipse as an occultation not of a jet but of a "corona" surrounding the accretion disk.

Finally, weak lines of an A-type star, a probable mass donor were discovered during eclipses in the spectra of SS 433 (Gies et al., 2002a). These lines are present in the blue spectral range. The lines of the A star are weak, its spectroscopic contribution in the mid-eclipse is estimated as 0.36 ± 0.07 in the V band (Hillwig & Gies, 2008). After this discovery, several attempts were made to determine masses of SS 433 components with the dynamic method, i.e. measuring amplitudes of the radial velocity curves, K_x and K_{opt}. The results are reviewed in Kubota et al. (2010). They are the following.

Source	M_x	M_{opt}	q
Gies et al. (2002a)	11 ± 5	19 ± 7	0.58
Gies et al. (2002b)	16.6 ± 6	23 ± 8	0.72
Hillwig et al. (2004)	2.9 ± 0.7	10.9 ± 3.1	0.27
Cherepashchuk et al. (2005)	18	24	0.75
Hillwig & Gies (2008)	4.3 ± 8	12.3 ± 3.3	0.35
Kubota et al. (2010)	$1.9 - 4.9$	$10.4^{+2.3}_{-1.9}$	$0.18 - 0.47$

However, Barnes et al. (2006) argued that the A-type supergiant spectrum may not be formed in the photosphere of the donor, it probably originates in the accretion disk wind. In such a case, the visibility of absorption lines should decrease in eclipse, but the reverse effect is observed. This is a good reason to believe that an A-type donor exists in the system.

Whatever the source, the donor or the wind, the data ambiguity concerning the components' masses reflects difficulties of the dynamic method. These difficulties are the following. With q as small as 0.15 and with a very hot radiation source heating the surface of the A-type star, we can observe the absorption-line spectrum only from the opposite side of the donor. The mass center of the system is located near the center of the donor, so actually we see the effect of donor's synchronous rotation, not the orbital motion. This effect leads to an overestimate of the amplitude of mass-center motion. Kubota et al. (2010) tried to account for this effect, and the lower limit of the mass estimate decreased to $1.9M_\odot$ as a result. With a simple model, they reduced K_{opt} to 40 ± 5 km s^{-1}. They conclude that "the compact object in SS 433 is most likely a low mass black hole, although the possibility of a massive neutron star cannot be firmly excluded". Otherwise, the mass of a neutron star may be close to the Chandrasekhar limit of $1.4M_\odot$ if SS 433 is a semidetached system with a heavy accretion disk (having a mass of $0.5M_\odot$), or, what is more probable, a contact system with an $0.5M_\odot$ star-like component having a neutron core (the Thorne & Zhitkov (1975, 1977) case). Certainly, one should take into account the presence of other matter in addition to the compact star in its Roche lobe in the system with a large rate of mass exchange.

Additionally, most authors used $K_{opt} = 175$ km s^{-1}, as measured by Fabrika & Bychkova (1990) on the base of the HeII 4686 Å line or $K_{opt} = 162$ km s^{-1} from Gies et al. (2002b), based on the CII 7231, 7236 Å blend. These emissions were attributed by the cited authors to the accretion disk surrounding the compact companion. This is a weak assumption. Typically, the HeII line has FWHM = 700 km s^{-1}, with wings to FWZI > 2600 km s^{-1}. In an eclipse, the equivalent width increases due to fainter continuum, so the largest part of the emission belongs to a nebular envelope surrounding the system but not to the accretion disk. Indeed, its shape is sometimes double-peaked. However, in an eclipse, we should expect, first, covering the blue peak from the approaching disk stream; then, covering the red peak from the recessing stream; and then, their

consequent recovering. Actually, the eclipse in HeII line goes otherwise. The blue wing of the line is eclipsed, and the line becomes narrower, what Goranskij et al. (1997) treat as an eclipse of a wide-angle conical outflow directed along the jet. Our analysis of the spectra by Kubota et al. (2010) taken in the eclipse on 2007 October 6 confirms this behavior of the HeII line. Thus, problems of dynamic mass determination for SS 433 are due to complex structure of lines that do not reflect the mass-center motion of the components.

Alternatively, we can find masses of the components in the system of SS 433 from the spectroscopic contribution of the A-type donor during an eclipse (36 ± 7 % in the V band). For the known upper limits of distance ($d \leq 5500$ pc) and interstellar extinction ($A_V \leq 8\overset{\mathrm{m}}{.}3$), we can calculate the lower limit of the donor's absolute magnitude, $M_V = -6\overset{\mathrm{m}}{.}2$, from a simple formula:

$$M_V = m_V + 5 - 5 \cdot \log_{10}(d) - A_V. \quad (4)$$

Based on the theoretical and observational mass-luminosity relations, such a star may have a mass of $11.7 M_\odot$. Then, the upper limit for the compact companion is $1.76 M_\odot$ taking into account $q = 0.15$, as derived from X-ray observations. Thus, the modern knowledge of SS 433 parameters currently seems to exclude the presence of a black hole in SS 433.

Nevertheless, I tried to verify and improve the modern data on mass ratio, interstellar extinction, photometric calibration using contemporary optical and X-ray observations. It is also of interest to estimate the contribution from the A-type donor using the photometric method.

2 ORBITAL PERIOD AND MASS RATIO

To check the mass ratio determined with the GINGA X-ray observatory, I used 79784 X-ray observations of RXTE/ASM in the $1.3 - 15$ keV energy range accumulated between 1996 January 5 and 2011 March 9 at the RXTE Internet site:

`http://xte.mit.edu/ASM_lc.html.`

These observations have a very low accuracy, but with the number of measurements that large, if averaged in orbital or precession phase bins, they allow us to establish the shapes of precession and eclipse light curves in this energy range. The orbital period was improved using our collection of photometric $UBVRI$ observations. The light curves and literature source list can be viewed with a Java-compatible browser at:

`http://jet.sao.ru/~goray/v1343aql.htm.`

The table of observations is accessible in the file:

`http://jet.sao.ru/~goray/SS.DAT.`

The first column of the Table contains Julian Dates of observations in the form of JD − 2400000.0; the next columns are respectively the V, B, U, R, and I magnitudes, with their source indicated in the last column. Note that the R and I magnitudes were taken both in Johnson and in Cousins systems, so the light levels are highly inconsistent. These observations were performed in the time range between 1978 October 5 and 2011 July 29, and the table is continuously replenished by new data.

The 35 best revised and new mid-eclipse times are given in Table 1. To determine these times, the eclipse light curves were superposed with the same, but mirrored, curves

in the PC screen; the axis of the mirror reflection was taken for the center of an eclipse. With these eclipse timings, the light ephemeris was determined using least squares fitting, with the following result:

$$\begin{array}{rlll} \text{Min I} = & \text{JD hel. } 2450023.746 & + 13^{\text{d}}.08223 & \cdot E. \\ & \pm.030 & \pm.00007 & \end{array} \tag{5}$$

The O−C curve calculated with this ephemeris is shown in Fig. 3 (top). Note that the deviations of individual minima from the ephemeris are larger than their mean errors. Figure 3 (bottom) demonstrates that these deviations do not depend on the precession phase. Precession phases ψ were calculated using the following ephemeris:

$$T_3 = \text{JD } 2449998.0 + 162^{\text{d}}.278 \cdot E. \tag{6}$$

Fitting the O−C curve with a quadratic expression reveals the quadratic term to be insignificant. This means that the orbital period did not vary between 1979 and 2007.

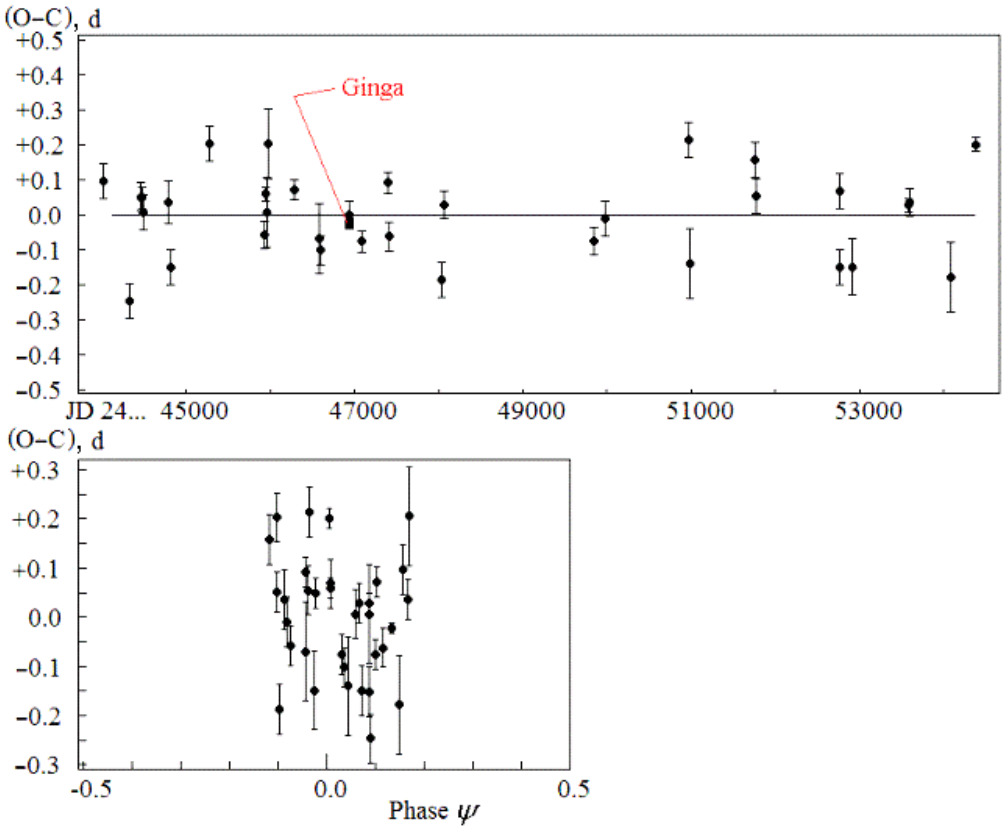

Figure 3. The O−C curve for the orbital period (top). Deviations of eclipse minima plotted versus phase of the precession period (bottom). No relation between them is visible.

The light curve for RXTE/ASM data in the $1.3 - 15$ keV energy range plotted versus phases ϕ of the orbital period calculated from eq. (5) is shown in Fig. 4 (top). The points deviating from zero by more than ± 10 cts s^{-1} were eliminated. Figure 4 (middle) demonstrates the same data plotted versus phases ψ of the precession period calculated with the formula (6). This is a mean light curve averaged by phase using the moving-average method, with a phase interval of 0.10. The curve indicates periodic variability of the X-ray flux in the range between 0.15 and 0.55 cts s^{-1}, i.e. by the factor of 3.7. Figure 4 (bottom) demonstrates the residuals revealed by prewhitening the data for the precession

wave, plotted versus the orbital-period phase again. The residuals were averaged by phase ϕ calculated from eq. (5) using the same moving-average method but with a smaller phase interval of 0.05. The mean orbital light curve shows the average flux constant in the phase range between 0.10 and 0.90, with a dip at phases between 0.90 and 0.10 due to the eclipse. The RXTE/ASM light curve is compared to the GINGA light curve for the eclipse on 1987 May 20 in Fig. 5. Taking into account a small systematic shift of the individual eclipse relative to averaged curve of multiple eclipses and smoothing the averaged curve with the width of average interval, one finds the agreement to be good enough. The RXTE/ASM data confirm that the eclipse is caused by covering the jet base, and the jet base is located as close to the donor's surface as follows from the mass ratio of $q = 0.15$.

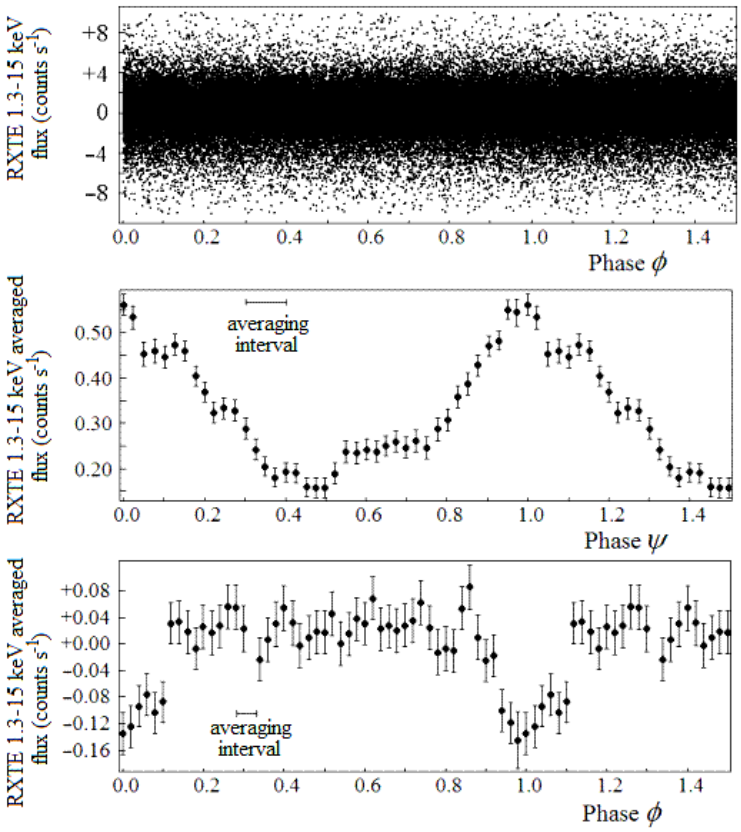

Figure 4. The RXTE/ASM X-ray phased light curves. Top: 79784 X-ray observations plotted versus the phase of the orbital 13.08223-day period. Middle: the averaged light curve calculated with the precession period of $162\overset{\mathrm{d}}{.}278$. Bottom: the averaged light curve for residuals after prewhitening the precession wave plotted versus the phase of the orbital period, $13\overset{\mathrm{d}}{.}08223$ days. The middle and bottom curves were calculated using the moving-average method, the averaging intervals are shown.

3 THE INTERSTELLAR EXTINCTION LAW

SS 433 is subject to strong extinction by interstellar medium. This extinction is a sum of absorption and scattering of the star light by the interstellar dust; physics of these processes is described by Savage & Mathys (1979). The V-band extinction of SS 433 light may reach 8 magnitudes. To estimate the absolute magnitude of the A-type donor of SS 433, we need to know both the accurate reddening $E(B-V)$ and the shape of the

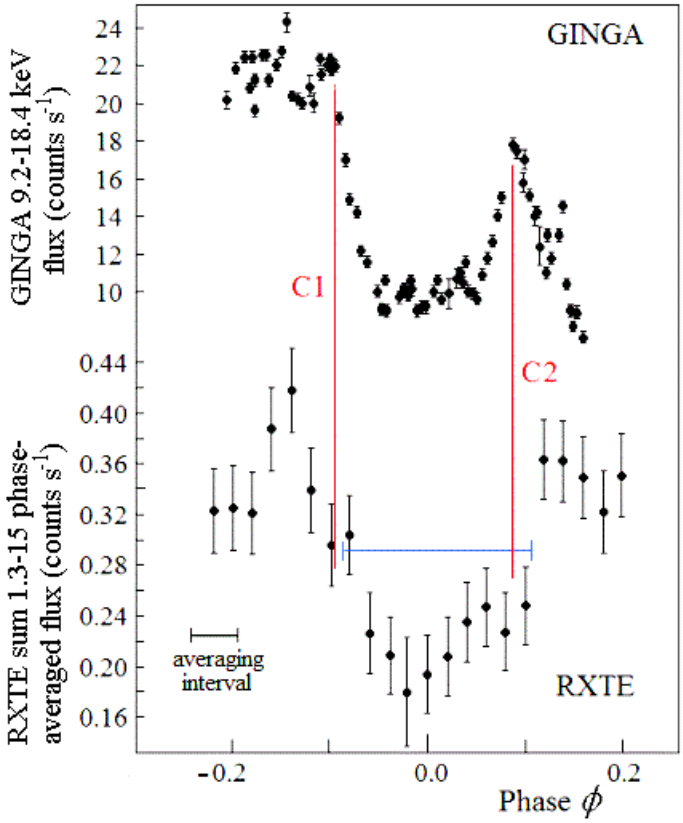

Figure 5. Comparison of X-ray eclipse light curve shapes. Top: the GINGA light curve for the eclipse on 1987 May 20. Bottom: the average eclipse light curve from RXTE/ASM data. $C1$ and $C2$ are phases of jet-base contacts with the donor's limb.

interstellar-extinction curve, $A_1(\lambda)$, normalized to unit reddening, $E(B-V) = 1.0$. The extinction curve was a subject of many studies; cf. the historical review in Straizys (1977). It was ascertained that the shape of the extinction curve varied in different directions and had different anomalies both in the near-ultraviolet and near-infrared ranges. Strong anomalies were found in the ultraviolet range in the nearby LMC and SMC galaxies. In Fig. 6, we compare the interstellar extinction law curves measured by J. Sudzius (published in Straizys, 1977) for the directions of Cepheus, Perseus, and Monoceros (converted from optical depths to magnitudes) to later-published curves by Schild (1977), Savage & Mathys (1979), Seaton (1979), Koorneef & Code (1981), Nandy et al. (1981), Howarth (1983), and Prevot et al. (1984). Most authors agree that $A_V = 3.08$ at $E(B-V) = 1.0$, but this value may be somewhat variable.

The formula to calculate interstellar extinction $A(\lambda)$ is:

$$A(\lambda) = A_1(\lambda) \cdot E(B-V). \tag{7}$$

Observations show some deviations in the U-band extinction law that can reach $0\overset{m}{.}8$. The largest deviation downward found in the ultraviolet is exhibited by the extinction curves in the LMC and SMC by Nandy et al. (1989), curve 5; Koornneef & Code (1981), curve 6; and Howarth (1983), curve 8a. Curve 8 by Howarth (1983), measured for the Galaxy, does not show a deviation that big. The largest deviation downward for the Galaxy is in the curve 6 by Schild (1977). This author found anomalous absorption below the Balmer jump in Perseus and in one region in Cygnus, but the normal law in the other Cygnus region. According to Galactic data, the dispersion of extinction curves in the UV

band in our Galaxy may reach $0\overset{m}{.}5$.

I have chosen the Savage & Mathys (1979) curve as a template to use for SS 433 because it is in the best agreement with other observations in the BVR spectral range and is frequently used in data reductions with the ESO MIDAS package. It should be taken into account that this table of extinction can have an insufficient accuracy when applied to reductions for a star as absorbed as SS 433.

Fortunately, there is a method to correct the individual extinction law for SS 433 on the base of multicolor photometry or spectrophotometry. Using observations of SS 433 during an eclipse, we can extract the spectrum of the very hot central source, which is covered in eclipses, from the combined light of the system. The combined light contains also the radiation from the surrounding gaseous shell and disk. We assume that the extracted spectrum is an extension of the thermal bremsstrahlung continuum that is radiated by the jet, its temperature being about $2.3 \cdot 10^8$ K (Yuan et al., 1995). The slope of such a spectrum in the wide wavelength range covering near-UV, optical, and near-IR domains is similar for temperatures exceeding 10^6 K. The extracted continuum can be used as a calibration standard to measure the extinction. The problem of extinction can be solved by comparison of the observed extracted spectral energy distribution to a calculated energy distribution for a black body with $T_{eff} = 10^6$ K.

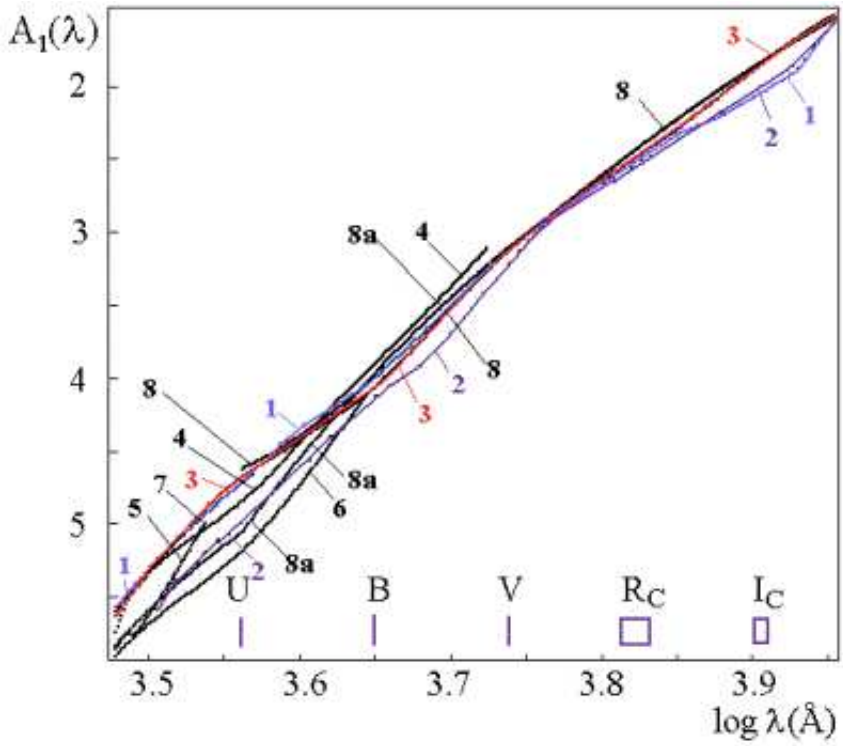

Figure 6. Curves of the interstellar extinction law measured in different studies. 1: Sudzius (Straizys, 1977); 2: Schild (1977); 3: Savage & Mathis (1979); 4: Prevot et al. (1984) for the SMC; 5: Nandy et al. (1989) for the LMC; 6: Koornneef & Code (1981) for the LMC, from observations with the IUE observatory; 7: Seaton (1979); 8: Howarth (1983) for the Galaxy; 8a: Howarth (1983) for the LMC. The extinction curve by Savage & Mathis (1979) (No. 3), plotted red, was chosen for this study.

4 OBSERVATIONS AND DATA REDUCTION

To analyze spectral energy distributions, I used multicolor CCD $UBVR_CI_C$ photometry of SS 433 in two eclipses centered at 2003 October 1 (JD 2452914.77; $\psi = 0.97$) and 2007 October 6 (JD 2454380.33; $\psi = 0.99$) from our collection mentioned in Section 2. The observations were made with the SAO 1-m Zeiss reflector and a photometer equipped with an EEV 42-40 chip and standard filters. Observations of the eclipse on 2007 October 6 were a part of a big campaign and accompanied with extensive spectroscopy using the Russian 6-m BTA telescope and the Japanese 8-meter Subaru telescope. The results of this campaign were published by Kubota et al. (2010). During spectroscopic observations with the Subaru telescope, a series of direct CCD frames with the V filter were acquired in order to point the star into the spectrograph slit. I reduced these frames and also used them for the analysis. Additionally, I used the BTA and Subaru spectroscopy to estimate the emission-line contribution in the photometric bands. The Subaru/FOCAS spectra are from four nights between 2007 October 6 and 10 and cover the wavelength range of $3750 - 5250$ Å with a dispersion of 0.37 Å per pixel. The BTA/SCORPIO spectra were taken on four nights between 2007 October 4 and 7 and cover the $3944 - 5705$ Å range with a dispersion of 0.86 Å per pixel.

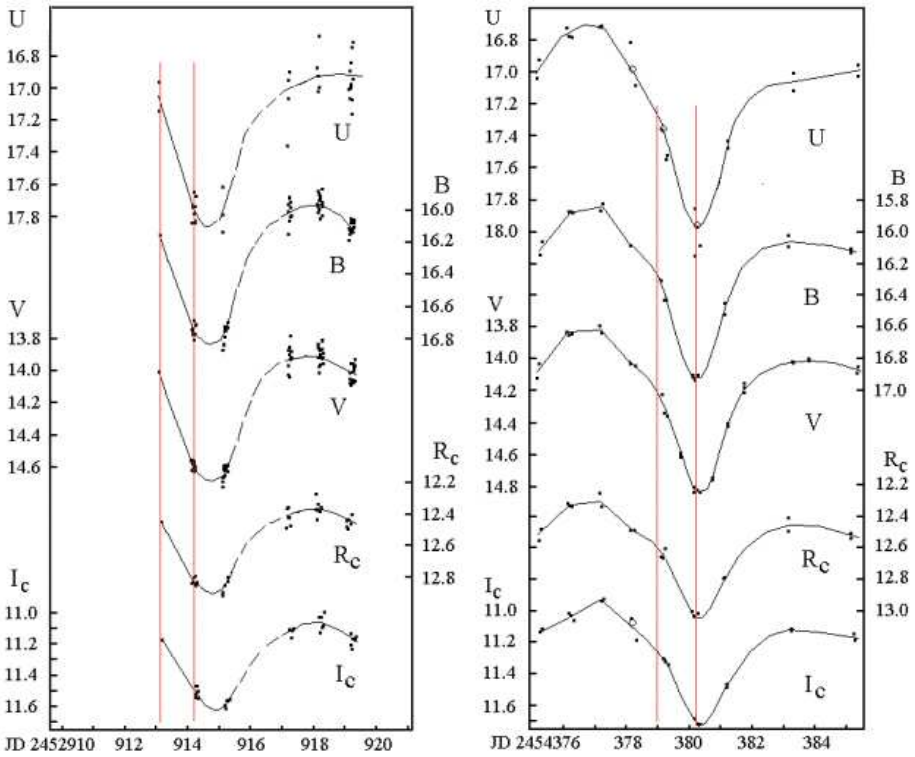

Figure 7. The light curves of two eclipses, on 2003 October 1 (left) and on 2007 October 6 (right), in the $UBVR_CI_C$ filters (arranged in the order of filter wavelength from top to bottom). The vertical red lines mark the phase interval of the ingress of the hot central light source. The light loss between these phases is used to extract the spectral energy distribution of the hot source with the difference method.

The CCD photometry was reduced in a standard way using bias and flat field frames. Dark frames were not applied because of deep freezing of the CCD chip with liquid nitrogen to a temperature of $-133°$ C. The thermal noise is negligible at this temperature. The nearby star Lyuty 9 (GSC 00471–00142), the southern star of the rhomb, was the

comparison star. The star has a faint red companion at $6''.0$ NE; its contribution to the combined light is significant in the V, R, and I bands in the cases of poor seeing. On such occasions, the comparison-star pixels affected with the companion were eliminated from the star profile, and their intensities were replaced with average-profile intensities when computing the integrated light. Extraction of images was performed with my software WinFITS in the aperture mode, with a star-profile correction. The $UBVR_CI_C$ magnitudes of the comparison star are respectively the following: 15.073, 14.581, 13.431, 12.973, 12.383. Additionally, four check stars were used. The uncertainty of the measurements is about $0^m.02 - 0^m.04$ in the BVR_CI_C filters, and about $0^m.1$ in the U filter. Generally, several observations were done on a night. The light curves of the two above-mentioned eclipses are shown in Fig. 7 for all the filters. In a few cases when nightly differences of measured magnitudes were sufficiently large, I co-added frames with matchimg star images and remeasured the nightly-sum frame. Such observations are marked with circles in the Figure.

As follows from the X-ray observations (Fig. 5), the ingress of the jet base begins at $\phi \approx 0.905$, the egress ends at $\phi \approx 0.095$ and the eclipse of the jet is partial. Near the jet base ingress, the optical light decline is most rapid. To extract the spectral energy distribution of the hot light source using the difference method, we should include phases $\phi = 0.905$ of both eclipses in the phase interval where the light loss of the hot source happens. These intervals are shown in Fig. 7 with vertical lines. In the eclipse on 2007 October 6, both ingress and egress were observed. The shape of the eclipse was symmetric, the light curve is well compatible with its reflected one. Therefore, I used both egress and ingress to measure the light lost in the eclipse. I interpolated magnitudes to include phases of the jet base contact. To compare the energy distribution of the light lost in the eclipse to the Planck energy distribution, we should transform magnitudes into physical units of erg $\mathrm{cm}^{-2}\mathrm{s}^{-1}\text{Å}^{-1}$.

5 ABSOLUTE CALIBRATION OF THE $UBVR_CI_C$ SYSTEM

It is known that the zero point of the $UBVR_CI_C$ photometric system is related to A0V stars. It is accepted by definition that all unreddened color indices of such star are zeros. Spectrophotometry deals with monochromatic intensities, i.e. intensities are measured in the physical units, and an element of spectral dispersion (pixel) is so small that intensity varies insignificantly between nearby elements. In the wide-band photometry, the width of transmission curve is usually thousands of Angströms, and stellar magnitudes are heterochromatic. In the spectral energy distribution measured with wide-band photometry, each magnitude corresponds to the mean wavelength of the device transmission curve $r(\lambda)$, calculated as:

$$\lambda_0 = \frac{\int r(\lambda)\lambda d\lambda}{\int r(\lambda) d\lambda} \tag{8}$$

(Straizys, 1977). The heterochromatic extinction is equal to the monochromatic extinction at the effective wavelength calculated as:

$$\lambda_{eff} = \frac{\int I(\lambda) r(\lambda)\lambda d\lambda}{\int I(\lambda) r(\lambda) d\lambda} \tag{9}$$

(King, 1952). $I(\lambda)$ is the monochromatic spectral energy distribution. Equation (9) means that the intensities measured with wide-band filters correspond, in the energy distribution, to λ_{eff} but not to λ_0. Replacing λ_0 with λ_{eff} for each filter and calculating intensities between filters for the wavelength set of the extinction curve with the linear interpolation

method, I tried to reduce the solution of the photometric problem to a spectrophotometric one.

Straizys (1977) used the calibration of UBV magnitudes from Straizys & Kuriliene (1975), based on the Vilnius photoelectric system. These calibration flux densities for a zero-magnitude A0V star are given in the fourth column of Table 2. The mean wavelengths λ_0 for the filters given in column 2 of this Table were calculated by me via eq. (8) using filter transmission curves presented in the digital form by Moro & Munari (2000). Moro & Munari give Vilnius coefficients along with another version of coefficients, which became popular and are called the photoelectric USA version (Matthews & Sandage, 1963). These UBV data along with the Cousins RI calibration coefficients are given in Column 5 of Table 2. Note that the reduction coefficients of the Vilnius and USA systems differ by 5.7 percents in the U band and by 8.6 percents in the B band, just in the spectral region where the strong multiple Balmer absorptions of an A0V star and its Balmer jump are located. Such a big uncertainty is inadmissible for SS 433 calibration.

Therefore, I examined the reduction coefficients of the $UBVR_CI_C$ system using Moro & Munari transmission curves with the modern spectral energy distribution of the A0V star Vega published by Bohlin & Gilliland (2004). The V magnitude of 0.026 ± 0.008 is established for Vega in the cited paper, and the absolute flux level is $3.46{\cdot}10^{-9}$ erg cm^{-2}s^{-1} at λ5556 Å. The reduction coefficients were calculated as average values of the Vega flux density weighted with the filter transmission curve, as follows from the formula:

$$f_\lambda = k \cdot \frac{\int FD_V(\lambda) r(\lambda) d\lambda}{\int r(\lambda) d\lambda}, \tag{10}$$

where $FD_V(\lambda)$ is the spectral energy distribution of Vega (flux density function), and $k = 10^{0.4 \cdot 0.026} = 1.024$ is the correction for the difference between the Vega V magnitude and zero. The calculated reduction coefficients are presented in the last, sixth column of Table 2. These coefficients may be used for normal stars with atomic absorption spectra. But they should not be used for cool stars with wide absorption bands or molecular emission, and certainly not for stars with such a big extinction as that of SS 433. Straizys (1977) noted that calibration coefficients for the wavelength between filters' mean wavelengths in the infrared range can be calculated by means of interpolation. However, my tests in the U and B spectral regions demonstrate that it is not true at short wavelengths due to multiple deep Balmer absorptions and the Balmer jump. Thus, for SS 433, I calculated special reduction coefficients not for filter transmission curves but for actually measured light, according to the expression:

$$f'_\lambda = k \cdot \frac{\int FD_V(\lambda) I_{SS}(\lambda) r(\lambda) d\lambda}{\int I_{SS}(\lambda) r(\lambda) d\lambda}, \tag{11}$$

where $I_{SS}(\lambda)$ is the first approximation for the SS 433 energy distribution calculated by interpolation, with normal reduction coefficients.

The results are given in Table 3, where the effective wavelengths of measured light are given in Column 2, their logarithms are in Column 3, and the "A0V-star zero-magnitude" reduction coefficients for these effective wavelengths are in Column 4. Comparison of Columns 2 in Tables 2 and 3 shows that the effective wavelengths in the short-wavelength filters differ from the mean wavelengths by about 200 Å, and this effect should be taken into account for SS 433.

The spectral energy distributions of SS 433 in the two eclipses, after such a correction but not yet corrected for interstellar extinction, are shown in Fig. 8. The results of energy-distribution correction for interstellar extinction made individually for both eclipses are

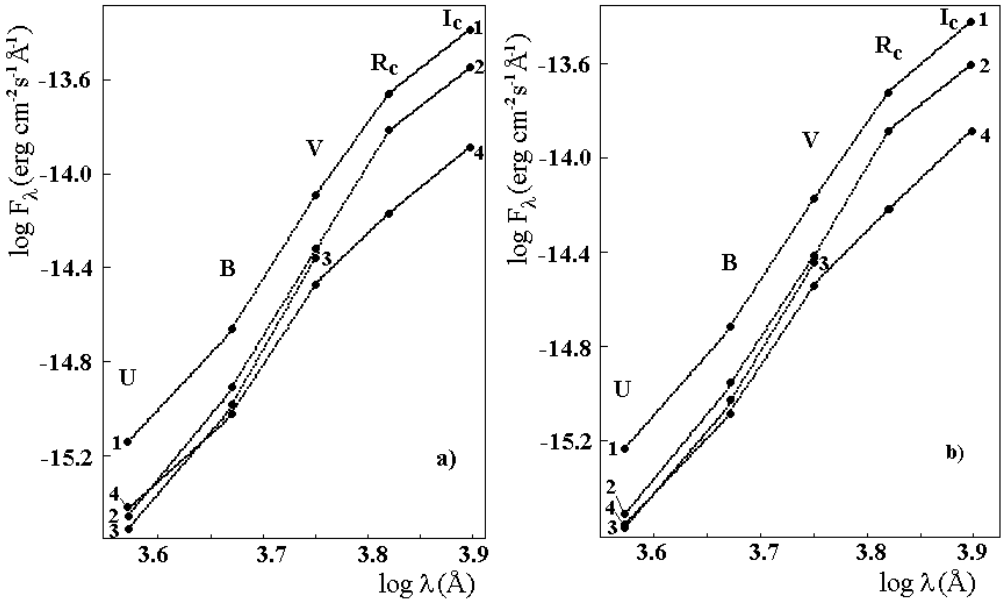

Figure 8. The spectral energy distributions of SS 433 in two eclipses, on 2003 October 1 (a) and on 2007 October 6 (b), not corrected for interstellar extinction. 1: The near-contact distribution, jet base included; 2: the distribution near the eclipse center, jet base covered; 3: the energy distribution in the UBV bands near the eclipse center, with the contribution from emission lines eliminated; 4: the energy distribution for light lost in the eclipse.

shown in Fig. 9. In Figs. 8 and 9, different energy distributions are plotted, those of light near the jet-base contact with the jet base included, those of light near the eclipse center with the jet base covered in the eclipse, and those of light lost in the eclipse. The distribution of the lost light is calculated as the difference of distributions with the jet base included and excluded. The correction for interstellar extinction was made by choosing a color excess value to get the best fitting, by eye, of the lost-light distribution (No. 3) with the black-body distribution for $T_e = 10^6$ K (the straight red line in Fig. 9). In such fitting, the level of black-body distribution was a free parameter, so a color excess was chosen only to fit its slope. With the photometry of 2003 October 1 eclipse, the best-fit color excess is $2\overset{\mathrm{m}}{.}62$, and for 2007 October 6 eclipse, it is $2\overset{\mathrm{m}}{.}68$. The average is $E(B-V) = 2\overset{\mathrm{m}}{.}65 \pm 0\overset{\mathrm{m}}{.}03$.

It is important to note that the strong excess in the R and I bands described above is revealed in every energy distribution of SS 433 being compared to the distribution of light lost in the eclipse. It is seen both in Fig. 8 in the reddened data and in Fig. 9 in unreddened data. The contribution of this excess can be easily extracted from the combined light. For this purpose, we extrapolate linearly the short-wavelength part of the combined-light distribution to the R and I bands and subtract the extrapolated values. However, the excess veils such a faint light source as an A-type star and makes its extraction impossible in the R and I bands.

The shape of the lost-light energy distribution, corrected for reddening with the determined $E(B-V)$, is nearly a straight line. This fact confirms my assumption on the nature of this light source as an optical tail of the energy distribution radiated by the jet bases. The maximum of this energy distribution is located far in X-rays. The individual points of the lost-light distribution indicate small deviations from the straight line in different filters (Fig. 9a,b), probably due to systematic errors in comparison-star magnitudes, uncertainties of the chosen extinction law, or inconsistency of the general law with the individual law in the particular sky direction, etc. Thus, the individual extinction law

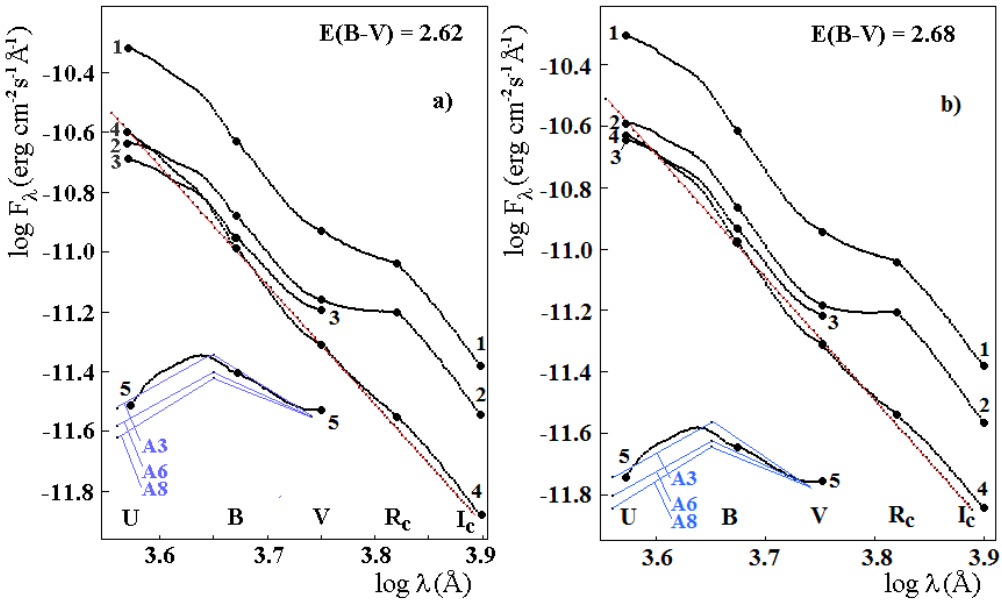

Figure 9. The spectral energy distributions of SS 433 in two eclipses, on 2003 October 1 (a) and on 2007 October 6 (b), corrected for interstellar extinction. Numbers $1-4$ indicate the same energy distributions as in Fig. 8. 5 is the extracted energy distribution of the donor. The straight red line is the Planck energy distribution for a black body with $T_e = 10^6$ K. The blue curves are unreddened photometric energy distributions for the stars HD 12027 (A3III), HD 240296 (A6III), and HD 12161 (A8III).

can be derived as the difference between the observed lost-light energy distribution and the selected calculated Planck energy distribution divided by the average of reddening.

If we adopt the light contribution of an A4–A8 donor between 0.29 and 0.43 in the eclipse in the V filter (Hillwig & Gies, 2008), and taking into account the earlier described parameters and uncertainties of distance and extinction, the absolute magnitude of the donor will be limited to $-6\overset{\mathrm{m}}{.}28 \leq M_V \leq -5\overset{\mathrm{m}}{.}40$. In the spectral type — absolute magnitude diagram (Fig. 10), the star occupies the uncertainty region plotted as a green rectangle. The radius of such a star can be calculated using the Stephan–Boltzmann law, $L = 4\pi R^2 \sigma T^4$, or, in solar units,

$$\frac{L}{L_\odot} = \left(\frac{R}{R_\odot}\right)^2 \cdot \left(\frac{T}{T_\odot}\right)^4. \qquad (12)$$

With this formula, the radius of the A-type donor can be estimated as 50–80 $R_\odot$. Naturally, with such a companion, we have no doubt in the "thin-jet" hypothesis when treating the X-ray eclipse. Otherwise, it is impossible to invent a collimation mechanism for the jet with the thickness of dozens of solar radii and with the collimation angle of 1.0–1.4 degrees by a compact object.

There is another question of interest. Can we detect, extract, or measure the contribution of the donor star during an eclipse from multicolor photometry knowing the possible range of its spectral type, A4–A8? The spectral energy distributions of SS 433 during eclipses (curves 2 in Fig. 9a,b) contain, besides the radiation from the donor, also the radiation from the hot source (possibly jet) eclipsed partially and the emission from the surrounding gas envelope, which may include also an equatorially expanding extended disk around the system described by Barnes et al. (2006, Fig. 1). Barnes et al. show that the donor is visible during the eclipse, near the precession phase $\psi \approx 0$, being not shielded

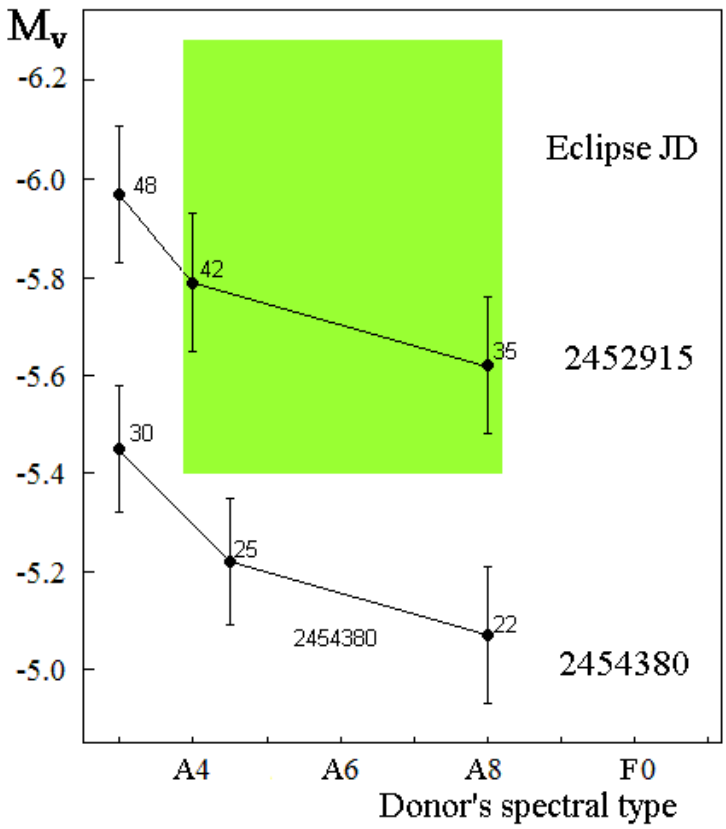

Figure 10. The spectral type – absolute V magnitude diagram. The green rectangle is the region of spectroscopic solutions. The points with error bars connected with broken lines are photometric solutions for the two eclipses. A number near each point is the contribution of the donor A star to the combined light of the system in eclipse.

by the extended disk. Using the Subaru and BTA spectra, I measured the emission contribution in the U, B, and V filters in the eclipse of 2007 October 6; the results are given in Table 4. The averages of these contributions to the UBV filters were subtracted from the intensities of light during eclipses (curves 2, Fig. 8 and 9), to get a pure continuum distribution in eclipses (curves 3). Note that the same emission-line contributions were subtracted also from the energy distribution of the 2003 October 1 eclipse because those observations were not accompanied by spectroscopy.

The unreddened UBV colors of HD 12027 (A3III), HD 240296 (A6III), and HD 12161 (A8III) were taken from Table 2 in Jacoby, Hunter, & Christian (1984) as examples of A-star colors. I plotted the spectral energy distributions of these stars in Fig. 9 as blue curves, for comparison, so that they intersect in the V-band range; the V-band intensity was used as a free parameter. Then I removed some portions of hot-source energy distributions (curves 4) from the eclipse-center energy distributions corrected for emission (curves 3), to find, in the residuals, an energy distribution resembling that of an A star (see curves 5 in Fig. 9). This is easy to do because a real star with a large Balmer jump is present in each of the two energy distributions. Accurately adjusting the subtracted hot-source energy distribution (curve 4) and the V-band intensity of the template, one can fit the residual distribution with any star, from A3 to A6. In the case of best fitting, V-band intensity of the sample corresponds to unreddened visible V magnitude of the donor. Certainly, the visible magnitude, absolute magnitude, and donor's contribution to the combined light (which is calculated for the V band) depend on

the energy distribution of the template chosen for fitting and on the amount of hot-source radiation. The results of residuals fitting are shown in Fig. 10 for each eclipse as points with error bars; the contribution of the A-type donor to the V band, estimated from each fitting and expressed in percents, is indicated by numbers near each point. It appears from Fig. 10 that the absolute magnitudes derived from photometry are systematically fainter than those derived from spectroscopy. Additionally, the derived absolute magnitudes of the donor change from eclipse to eclipse, so that their error bars do not overlap. The nature of these systematical differences is not yet clear. Using the two eclipses, we find the following absolute-magnitude limits: $-5\overset{\mathrm{m}}{.}9 \leq M_V \leq -5\overset{\mathrm{m}}{.}0$, for the donor spectra in the A4–A8 range.

6 THE MASS–LUMINOSITY RELATION

The Russell–Vogt theorem states that if we know a star's mass and its chemical composition, then, using laws of physics, we can determine all of its other properties, such as luminosity, radius, temperature and density profiles, and find how these properties change with time (Massey & Meyer, 2001). A. Eddington was the first to demonstrate that radiative diffusion in stars required a dependence of the stellar luminosity on mass, $L \sim M^4$. Since Eddington times, stellar luminosities are known from evolutionary modeling. Modeling shows a good mass–luminosity relation for main-sequence stars with hydrogen burning in their centers. But low-mass stars, like those in globular clusters, can reach high luminosities during late stages of their evolution, for example, the stage of a red giant with a degenerate helium core or the stage of an AGB star with a degenarate carbon core. Such stars deviate far from the general relation though for a comparatively short time. Other unaccounted effects in this theory, like rotation or binarity, can lead to violations of the relationship.

Star masses can be determined from observations if we apply dynamic methods to visual, eclipsing, or spectroscopic binaries, mostly detached systems. Certainly, the knowledge of accurate distances and luminosities is needed for such systems. Using this method for semidetached or contact binaries faces the problems described in this paper for the case of SS 433. Besides, it is possible to estimate a star's mass from high-resolution spectroscopy and stellar-atmosphere modeling. Fitting the observed line profiles to model ones gives the effective temperature T_{eff} and surface gravity g. If the star's distance and luminosity are known, one can calculate its radius from the Stephan–Boltzmann law (cf. eq. (12)), and then its mass from the relation $g \sim M/R^2$ (Massey & Meyer, 2001).

I analyzed the mass–luminosity relation for A-type stars using the evolutionary models by Schaller et al. (1992), specifically their evolutionary tracks for a nearly-solar chemical composition (Y = 0.30, Z = 0.020, their Fig. 1). Massive and luminous stars became A stars on their tracks to red giants. The evolution of massive stars to the red side of the C-M diagram goes at a constant luminosity, and hence the theoretical mass–luminosity relation is determined correctly, with an insignificant dispersion. The theoretical mass–luminosity relation for A stars is presented in Table 5. In Fig. 11, this relation is plotted over a fragment of the mass–luminosity diagram presented in Fig. 1 of Massey & Meyer (2001), which was constructed for components of binary stars. The relation for A stars is plotted as red points and a red broken line; the red numbers are initial masses of the models. Along the abscissa, current masses of A-star models are plotted: stellar models were computed with the mass loss taken into account. In the luminosity ranges of interest, the mass loss of single stars that become A stars varies from $0.013M_\odot$ for the initial mass of $9M_\odot$ to $0.10M_\odot$ for $12M_\odot$. Figure 11 shows that the A-star relation coincides with the

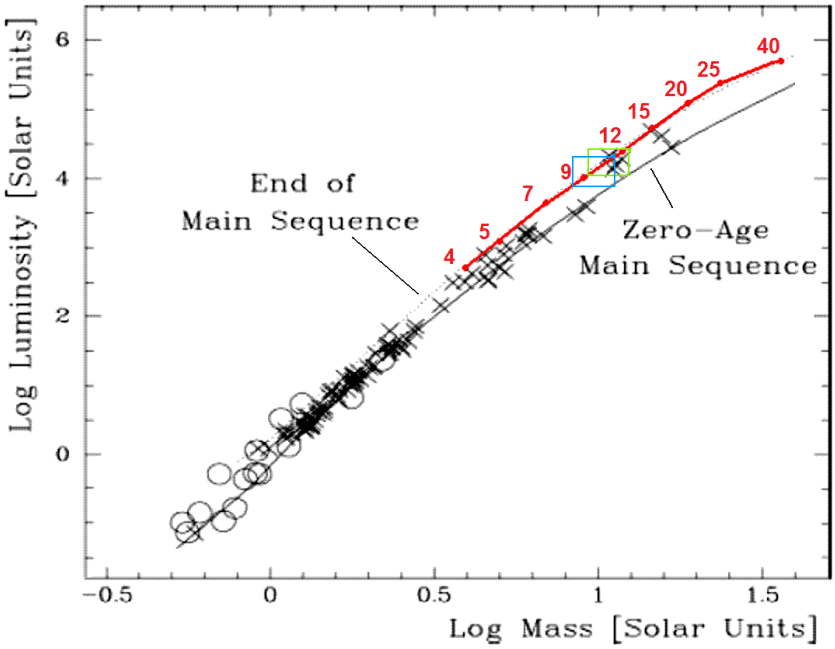

Figure 11. A fragment of the mass–luminosity diagram by Massey & Meyer (2001, Fig. 1) constructed for components of binary stars. The theoretical mass–luminosity relation derived by the author for A stars using the models by Schaller et al. (1992) is also plotted (red points and lines). There is an agreement with observations of binary components. The localization of SS 433 A-type donor is marked with two error boxes, the green box being the localization revealed from spectroscopy and the blue box, from photometry.

location of stars at the end of the main sequence, whereas the stars on the zero-age main sequence have larger masses for their luminosities. Our comparison of the theory with observations of star-system components reveals a good agreement.

SS 433 is not a single star, and the donor is losing mass at a higher rate than a single star, but the current bolometric luminosity of the donor should reflect its current mass. Principally, the bolometric absolute magnitude does not depend on the star's spectrum (or on T_{eff} on its surface), it depends on the energy release in the stellar interior. Eventually, however, the energy release depends on stellar mass.

When using the theoretical relationship for A stars to estimate the donor mass in SS 433, the question arises if this star has an internal structure similar to normal single stars with the same spectral types and luminosities. Actually, the volume of a star in a binary system is limited by the critical equipotential surface. A component of a binary evolving to the stage of degenerate helium core would not be able to become a red giant because its expanding envelope will overflow to the secondary component or flow away from the system. Such phenomena are observed in SS 433. A star with a forming helium core may have excess luminosity compared to a single star of the same mass. Using the relation for single stars, we will overestimate the mass of such a component. A common-envelope phase in a binary with an expanding component is also possible, and this can be just the case for the system of SS 433.

For masses exceeding $7M_{\odot}$, loops of evolutionary tracks occurring in the He-burning phase get into the region of A stars at somewhat higher luminosities than the luminosity on the way to red giants. The He-burning phase on such a loop seems improbable for the SS 433 donor. However, using the mass–luminosity relation for A stars in such a case, we will also overestimate the mass of the SS 433 donor. This means that if we use the

mass–luminosity relation for A stars derived using tracks to red giants but the real A star is at a later evolutionary stage and its envelope is limited by the binary's equipotential surface, then its mass will actually be lower, and lower will be the mass of the compact object.

The donor's mass determined from this relation, in agreement with its light contribution estimated spectroscopically, falls in the range from 9.4 to $12.5 M_\odot$, while the mass estimated photometrically is between 8.3 and $11.0 M_\odot$. The error boxes of the parameters derived for the donor are shown in Fig. 11 as rectangles. The green rectangle corresponds to the spectroscopically determined contribution in eclipse, and the blue rectangle corresponds to that determined photometrically. The location of the error boxes is in agreement with models for evolved stars that leaved the main sequence.

The mass M_X of the compact object can be calculated using the formula $M_X = qM_A$, where M_A is the mass of the A-type donor and $q = M_X/M_A = 0.15$ is the mass ratio known from observations of the jet eclipse in X-rays.

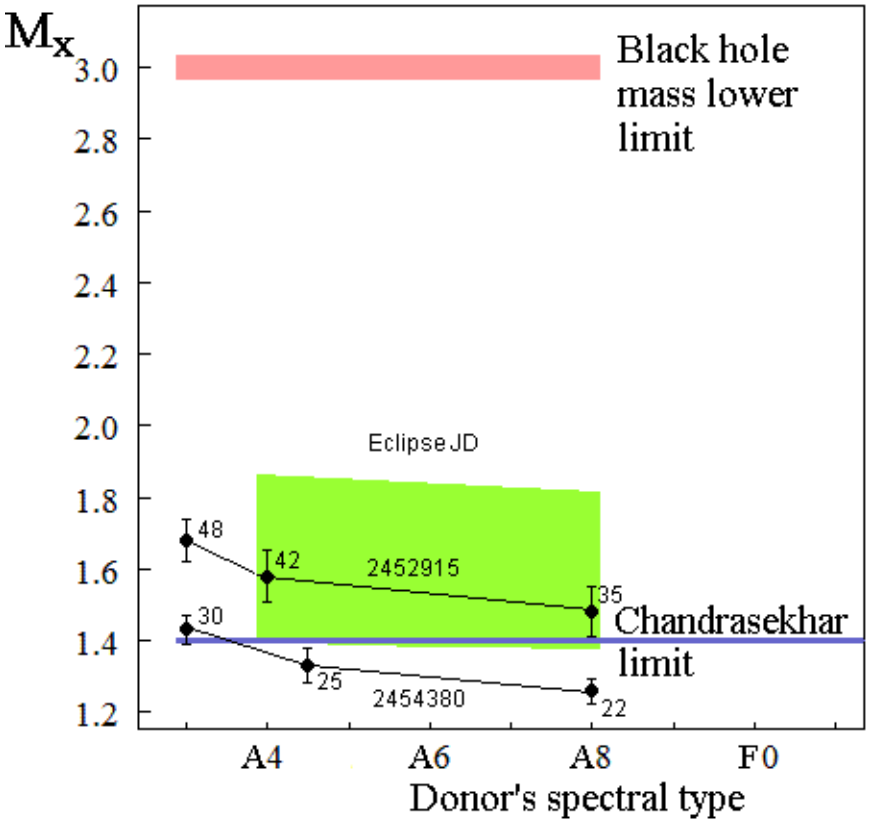

Figure 12. Mass estimates for the compact object based on the estimates of A-type donor luminosities. As in Fig. 10, the green rectangle is the region of spectroscopic solutions. Points with error bars connected with broken lines are photometric solutions for the mass revealed from photometry of the two eclipses. A number printed near each point is the V-band contribution (in percents) of the A-type donor to the combined light of the system in eclipse.

Now, having in mind all these considerations and using the small bolometric corrections, in the range between $-0\overset{\mathrm{m}}{.}05$ and $+0\overset{\mathrm{m}}{.}09$, respectively for A4I–III and A8I–III, we translate all the regions and points shown in Fig. 10 (the spectral type–M_V diagram) to the donor's spectral type–compact-object mass diagram for SS 433 (Fig. 12).

Figure 12 demonstrates that all mass estimates are concentrated near the level of

the Chandrasekhar limit established for zero-age neutron stars, $1.4M_{\odot}$ (blue line), but essentially below the lower mass limit for stellar-mass black holes, $3M_{\odot}$ (red line). Note that wrong identification of the donor's evolutionary stage would lead to smaller mass estimates for the compact component, and its mass will still be below the Chandrasekhar limit.

Our final mass estimates for the compact object in SS 433 are $1.64 \pm 0.23M_{\odot}$ for the donor's light contribution in the eclipse near T_3 derived spectroscopically and $1.45 \pm 0.20M_{\odot}$ for that derived photometrically and based on the donor's spectral type estimated from spectroscopy as A4 − A8 I−III.

To check if the masses of the components of SS 433 agree with laws of physics, let us calculate the amplitudes of radial-velocity curves K_A for the A-type donor and K_X for the compact object from the formulae of Keplerian dynamics:

$$f_X(M) = \frac{M_X^3 \cdot sin^3 i}{(M_X + M_A)^2} = 10385 \cdot 10^{-11}(1 - e^2)^{\frac{3}{2}} \cdot K_A^3 \cdot P, \tag{13}$$

$$\frac{K_A}{K_X} = \frac{M_X}{M_A}, \tag{14}$$

where M_A and M_X are respectively the masses of the A-type donor and the compact object; e is the orbital excentricity, assumed to be zero; i is the orbital inclination, $78\overset{\circ}{.}81$; P is the orbital period, $13\overset{\mathrm{d}}{.}08223$. The results are the following: $K_A = 26$ km s^{-1}, $K_X = 170$ km s^{-1}. Thus, the velocity-curve amplitude of the A-type donor is really 1.5 times smaller than the same parameter in Kubota et al. (2010), even that corrected for the heating effect, 40 km s^{-1}. At the same time, the velocity-curve amplitude of the compact component is well in compliance with the amplitudes revealed from the He II emission line, 175 km s^{-1} (Fabrika & Bychkova, 1990), or from the CII emission blend, 162 km s^{-1} (Gies et al., 2002b).

Let us now conversely calculate the magnitude of the donor star using the mass of $4.3M_{\odot}$ for the compact object from Kubota et al. (2010) and $3.0M_{\odot}$, the mass of a hypothetical black hole at the lower limit of black-hole masses. With the mass ratio $q = 0.15$ and the mass–luminosity relation deduced from Shaller et al. (1992), I estimated masses, absolute V magnitudes, and V-band visible reddened magnitudes of the A-type donor stars as respectively 28.7 and $20M_{\odot}$, $-9\overset{\mathrm{m}}{.}13$ and $-8\overset{\mathrm{m}}{.}25$, $12\overset{\mathrm{m}}{.}67$ and $13\overset{\mathrm{m}}{.}55$. Note that SS 433 has a maximum normal brightness of $13\overset{\mathrm{m}}{.}9$–$14\overset{\mathrm{m}}{.}0$ in the V band, and its brightness reaches $13\overset{\mathrm{m}}{.}55$ only in outbursts. This is the combined brightness of all components and light sources in the binary. Thus, black-hole masses are in a strong conflict with the results of photometry.

7 DISCUSSION

The general parameters used in this paper, such as distance, extinction, A-star contribution during eclipses near the T_3 precession phase are no surprise. They were repeatedly examined in different studies. The contribution of the A-type donor measured in this paper, 32 ± 10 percents in the V band, photometrically corresponds to a magnitude between 15.7 and 16.4. This range is in conflict with the magnitude of 17.35 in the V band measured in an eclipse, at the T_2 phase, by Henson et al. (1982). However, this contradiction can be easily understood if we remember the circumbinary equatorial expanding and precessing disk, well illustrated by Barnes et al. (2006), which covers the system partly in the precession phases near T_1 and T_2. The known dependence of eclipse depth on the precession phase with the amplitude of $0\overset{\mathrm{m}}{.}40$ can be explained with this disk, too. The

eclipse observed by Henson et al. was monitored also by Gladyshev et al. (1987), and it is known that, $0\overset{d}{.}5$ before and $0\overset{d}{.}5$ after the observation by Henson et al., the brightness of SS 433 was extraordinary high for those orbital and precession phases, so the object was in a high state. Probably, a time was caught when the circumbinary disk was extraordinary thick and covered the donor totally. This event could coincide with a short-duration weakening of the jets. Such an event was unique but observationally well established.

The nature of the circumbinary disk remains unclear yet. It is observed in radio bands as a wind of rapidly varying shape at the distances of about 200–250 AU and is resolved (Paragi et al., 1999). This structure is perpendicular to radio jets. The radio structure is discussed in detail in the review by Fabrika (2004); see additional references there. The disk may be formed by gas flowing out from the external Lagrangian point L2. It is unclear why this gas, which covers the central jet bases, does not form an absorption-line spectrum in the optical bands.

With the A-star contribution of 32 ± 10 percents in the V band in minimum light, its contribution is only 10–20 percents in maximum light. It is clear from an inspection of Fig. 2, where the light curve near T_3 has a β-Lyrae-like shape with a large-amplitude "ellipsoidal effect" and a secondary eclipse $0\overset{m}{.}4$ deep, that neither the ellipsoidal effect no the secondary eclipse can be related to the donor because of its small light contribution. The main bright source in the V band is the very hot one, covered partially in the primary eclipse. Then its contribution in maximum light is up to 77–87 percents, taking into account the 3-percent contribution of the emission-line-radiating envelope. If this is a hot disk or another rapidly rotating body, it also cannot form either the ellipsoidal effect or the deep secondary eclipse. Otherwise, the source may be a star filling the Roche lobe of the compact component and having an elongated shape due to the gravitational influence of the donor. Thus, the hypothesis of a "supercritical accretion disk" in SS 433 is a myth, and it is not confirmed with the photometry. It is not correct to fit the optical light curves by a model of a thick precessing disk plus a gravitationally distorted OB star, as that was done by Antokhina & Cherepashchuk (1985, 1987). Moreover, we do not see any details in the photometry that could be treated as external contacts of a bright star filling the Roche lobe of the compact component, though we know that the eclipse of the Roche lobe is total due to the small ratio, $q = 0.15$. No contribution of such a star, which may have an energy distribution different from that of the very hot source, is also detectable in multicolor photometry. It is small compared to the A-type donor contribution.

In such a case, we may expect that the light distribution of the hot source in SS 433 is formed only by jet bases and holes or nozzles the jets come from. The "ellipsoidal effect", the precession light variations, and the "secondary eclipse" of the very hot light source are present only due to effects of visibility of the nozzle depths and jets' bases. Near precession phases T_1 and T_2, the dispersion of light curves increases strongly (Fig. 2); the causes of this phenomenon may be both the system being covered by the nonuniform structure of the hypothetical circumbinary disk and variations of visibility conditions of nozzle depths due to uneven and rough structure of nozzles' edges. The hypothesis that the light curves of SS 433 could be explained by the motion of two bright hot spots at the points of emergence of the jets (or jet nozzles), while the contribution of the disk or its envelope to the total brightness was small, was first put toward by Lipunov & Shakura (1982).

Another important factor in forming the optical light curve can be variable brightness of jets. Hydrogen burning on the surface of a neutron star is very unstable, because a critical mass should be accumulated repeatedly for the ignition. Repeated ignitions may be the cause of forming the bullets. Appearance of bullets in the moving Balmer

lines means that the matter of jets is thrown out in portions. The connection of the bullet formation to the optical variations has not yet been studied. However, this effect can cause deviations of individual minima from the linear ephemeris found in my study. Additionally, the jets are driven by tidal waves responsible for nodding motion. Fourier analysis of our photometry also shows a significant wave with an amplitude of about $0\overset{m}{.}2$ and the same period as that of nodding motion of the moving H_α components in the spectra, $6\overset{d}{.}2887$ (Goranskij et al., 1998a).

I assume that, in the case of a contact system in SS 433 having a neutron star in the center of a component filling the Roche lobe, the products of hydrogen burning on the surface of the neutron star are channelling out of the star through the nozzles throwing most of the thermonuclear energy into space. Therefore, the surface of such a star with the neutron star inside can be heated insufficiently to contribute to the common light of the system. I think that cases of supercritical accretion on a black hole and of hydrogen burning on the surface of a neutron star differ in the chemical composition of matter erupted in jets. Indeed, no thermonuclear burning is possible if the matter falls into a black hole. It should be also reminded that Lipunov & Shakura (1982) demonstrated the liberation of energy through the accretion process on a neutron star to be the only process capable of explaining the energy release of SS 433.

The conclusions of this study are strongly dependent on the mass ratio $q = 0.15$ established from X-ray observations of the Ginga satellite. I assume that it is a very reliable result because the eclipse contacts were observed not only in continuum radiation but also in the moving emission blend of Fe XXV/Fe XXVI radiated by the jets. This circumstance permits to correctly localize the eclipsed source. The contacts and width of the X-ray eclipse are confirmed with the X-ray observations in continuum. Another confirmation of the mass ratio being so small is the radial velocity of the stationary H_α line, which is displaced by 90 degrees in orbital phase. The maximum recessive velocity in H_α is observed in the inferior conjunction of the donor, i.e. in eclipse. The equivalent width of the H_α line increases in eclipse due to deep eclipse in continuum, but the intensity of the line does not show any eclipse. This means that the line is radiated in an extensive and expanding envelope.

Goranskij et al. (1997) found a natural explanation for this phenomenon. In this system, a part of the envelope is located in a shadow of the companion. The companion covers the radiation of the hot source for the shadow cone, gas in the shadow rapidly recombines, and it cannot be excited by the hot source for the eclipse duration. The opposite side of the A-type donor, which has strong and wide Balmer and Lyman absorption lines, is not able to effectively excite the hydrogen in the shadow. The angle of the shadow cone, the volume of neutral gas in the envelope, the lost emission intensity, due to the shadow, in the line profiles, and the amplitude of the velocity curve based on mean-profile intensity variations depend strongly on the distance of the hot exciting source from the donor's surface, and therefore on the mass ratio q. My simple profile modeling with the Monte Carlo method shows that the observed amplitude of 160 km s^{-1} is best fitted with the mass ratio $q = 0.15$. Thus, the displacement of the H_α radial velocity curve is an additional argument in favor of a low mass ratio and low mass of the compact component.

Kubota et al. (2010) try to disprove this argument restricting it only to "wind evacuation", i.e. to covering the wind cone by the donor, with the wind being formed by the accretion disk. They thought this covering led to an anisotropic wind. Their arguments against the shadow hypothesis are weak. The first one is that the radial velocity amplitudes of H and HeI have to exceed those of the accretion disk (traced by the HeII line) since the disk powers the wind. The presence of such a disk has not yet been proven, the most questionable is the hypothesis of forming the HeII line by the disk. The behavior of

the HeII line in eclipse described above does not confirm its relation to the disk. No partial or total eclipses in H and HeI emission have been observed yet. Different amplitudes of H and HeI lines can be explained with different excitation conditions: the A-type donor has much weaker lines of HeI than those of H, and HeI atoms can be excited with a larger probability. The second argument is related to the accretion gas stream. If a gas stream drawn in the sketch in Fig. 13 in Kubota et al. (2010) really exists, it should be located near the L1 Lagrangian point between the stars and thus should be totally eclipsed in the phase range wider than that of the jet-base eclipse because the L1 Lagrangian point is closer to the donor than the jet bases. Even if located in the drawn place, the gas stream should be eclipsed totally but in the different range of orbital phases. Nothing of this behavior was observed. Additionally, H_α has a wide profile with FWHM $\approx$ 1500 Å, corrected for instrumental resolution in the spectra, so one should find a hypothetical stream component in the profile formed by the expanding wind with the velocity of about 750 km s^{-1} and exhibiting wide eclipses. Recently, Bowler (2009) detected a transient component in the profile of the H_α emission, subject to Doppler effect with the orbital period, at a speed of approximately 175 km s^{-1}, but this component is not eclipsed at any orbital phase (the mass he estimated for the compact object is less than $37M_\odot$). Bowler attributes this component to the accretion disk around the compact companion.

Thus, there exists additional evidence for a very small mass ratio for the components of SS 433 besides the Ginga X-ray observations in eclipses. Since Ginga times, new perfect X-ray observatories and devices have been launched into space and work successfully. One of such observatories is Chandra. Its HETGS spectrograph has a higher resolution and sensitivity than that of Ginga. In variance with Ginga, this device resolves the FeXXV/FeXXVI blend at 6 keV (Marshall et al., 2002). The Chandra team did not repeat the Ginga experiment aimed at detecting jet contact times during eclipses, but public releases at the Chandra Internet site are full with declarations that SS 433 is a black-hole binary. Why not check Ginga data with the modern Chandra observations?

Another problem which may have an improved solution is the mass − luminosity relation for A-type stars with high accretion rate caused by the evolution with the Roche-lobe-limited envelopes. In this study, it was naturally supposed that A-type stars that had lost their mass from the envelope evolved as single stars but with a smaller, residual mass. But it is of interest to solve this problem by modeling. It seems that this problem is not so difficult.

As a critical reader of my paper may note, I used, in Section 2, the filter transmission curves collected by Moro & Munari (2000) for the original Johnson and Cousins photometric systems, but not those for the instrumental $UBVR_CI_C$ bands used in our measurements with the SAO 1-m telescope. Accurate studies of such curves for the instrumental systems need special devices, like a a monochromator, and techniques of high-precision photometry described by Mironov (2008). Additionally, my experience shows that high-precision CCD photometry also needs special measures to prevent flashes originating from skew light reflection on the surfaces parallel to the optical axis of the telescope, such as the Cassegrain blend or cylindrical photometer details, even blackened. For precise CCD photometry, it would be preferable to have a special photometric telescope with a CCD detector in the prime focus, without any blend. However, we have to use multi-purpose telescopes, not prepared specially for precise photometry. This certainly affects adversely the accuracy of flat-field calibration and standard measurements. The absence of spectroscopy in the red spectral range is another perceptible drawback of this study. We used the available data as is. Performing absolutely correct photometry of SS 433, supported with spectroscopy with big telescopes, seems a difficult problem.

The best solution of this problem seems to be spectrophotometry with a wide and long

slit to prevent light losses at the slit, but at the cost of spectral resolution. Such observations require spectrophotometric standards in the close vicinity of SS 433. However, establishing such standards is not a difficult problem.

8 CONCLUSIONS

In this paper, it is reliably established on the base of current knowledge of distance, extinction, mass ratio, and contribution of A-type star for SS 433, along with modern data on stellar photomery, its physical calibration, stellar bolometric corrections, temperature calibrations, mass–luminosity ratio that the compact object in the system of SS 433 is a neutron star with a mass close to the Chandrasekhar limit, $1.4M_{\odot}$. This conclusion follows from the discovery of an A4–A8I–III star in the spectrum. With all possible estimates of the A-star's contribution to the combined light of the system during the eclipse, the mass of the neutron star is in the range between 1.25 and $1.87M_{\odot}$. The mass of the neutron star is $1.45 \pm 0.20M_{\odot}$ solely from multicolor photometry.

To adopt the assumption of a black hole, the basic parameters of SS 433 and main astrophysical data should be radically revised.

Acknowledgments:

The author thanks A.V. Mironov (Sternberg Astronomical Institute, Moscow University) for his help in some questions of stellar photometry and its calibration.

References:

Antokhina, E. A., Cherepashchuk, A. M., 1985, *Soviet Astron. Letters*, **11**, 4
Antokhina, E. A., Cherepashchuk, A. M., 1987, *Soviet Astron.*, **31**, 295
Aslanov, A. A., Cherepashchuk, A. M., Goranskij, V. P., et al., 1993, *Astron. & Astrophys.*, **270**, 200
Barnes, A. D., Casares, J., Charles, P. A., et al., 2006, *Monthly Not. Roy. Astron. Soc.*, **365**, 296
Blundell, K. M., Bowler, M. G., 2004, *Astrophys. J.*, **616**, L159
Bohlin, R. C., Gilliland, R. L., 2004, *Astron. J.*, **127**, 3508
Borisov, N. V., Fabrika, S. N., 1987, *Soviet Astron. Letters*, **13**, 200
Bowler, M. G., 2009, *arXiv*:0912.2428
Brinkmann, W., Kawai, N., Matsuoka, M., 1989, *Astron. & Astrophys.*, **218**, L13
Brinkmann, W., Kotani, T., Kawai, N., 2005, *Astron. & Astrophys.*, **431**, 575
Cherepashchuk, A. M., 1981, *Monthly Not. Roy. Astron. Soc.*, **194**, 761
Cherepashchuk, A. M., Aslanov, A. A., Kornilov, V. G., 1982, *Soviet Astron.*, **26**, 697
Cherepashchuk, A. M., Sunyaev, R. A., Fabrika, S. N., et al., 2005, *Astron. & Astrophys.*, **437**, 561
Crampton, D., Hutchings, J. B., 1981, *Astrophys. J.*, **251**, 604
Davydov, V. V., Esipov, V. F., Cherepashchuk, A. M., 2008, *Astron. Reports*, **52**, 487
Fabrika, S. N., 2004, *Astrophys. & Space Phys. Rev.*, **12**, 1
Fabrika, S. N., Bychkova, L. V., 1990, *Astron. & Astrophys.*, **240**, L5
Fejes, I., 1986, *Astron. & Astrophys.*, **168**, 69
Gies, D. R., Huang, W., McSwain, M. V., 2002a, *Astrophys. J.*, **578**, L67
Gies, D. R., McSwain, M. V., Riddle, R. L., et al., 2002b, *Astrophys. J.*, **566**, 1069
Gladyshev, S. A., Goranskij, V. P., Kurochkin, N. E., Cherepashchuk, A. M., 1980, *Astron. Tsirkulyar*, No. 1145

Gladyshev, S. A., 1981, *Sov. Astron. Letters*, **7**, 330
Gladyshev, S. A., Goranskij, V. P. Cherepashchuk, A. M., 1987, *Soviet Astron.*, **31**, 541
Goranskii, V. P., Fabrika, S. N., Rakhimov, V. Yu., et al., 1997, *Astron. Reports*, **41**, 656
Goranskii, V. P., Esipov, V. F., Cherepashchuk, A. M., 1998a, *Astron. Reports*, **42**, 209
Goranskii, V. P., Esipov, V. F., Cherepashchuk, A. M. 1998b, *Astron. Reports*, **42**, 336
Goranskij, V. P., 1998c, in: *Proc. of the 20-th Conference on Variable Star Research*, ed. J. Dushek, M. Zejda, Brno, Czech Republic, p.103
Grandi, S. A., Stone, R. P. S., 1982, *Publ. Astron. Soc. Pacific*, **94**, 80
Henson, G., Kemp, J., Krauss, D., 1982, *IAU Circ.*, No. 3750
Hillwig, T. C., Gies, D. R., Huang, W., McSwain, M. V., et al., 2004, *Astrophys. J.*, **615**, 422
Hillwig, T. C., Gies, D. R., 2008, *Astrophys. J.*, **676**, L37
Hjellming, R. M., Johnston, K. J., 1982, In: *Extragalactic radio sources*, Proceedings of the IAU Symposium No. 97, Dordrecht, D. Reidel Publishing Co. p. 197
Howarth, J. D., 1983, *Monthly Not. Roy. Astron. Soc.*, **203**, 301
Jacoby, G. H., Hunter, D. A., Christian, C. A., 1984, *Astrophys. J. Suppl.*, **56**, 257
Kawai, N., Matsuoka, M., Pan, H.-C., Stewart, G. C., 1989, *Publ. Astron. Soc. Japan*, **41**, 461
Kemp, J. C., Henson, G. D., Kraus, D. J., et al., 1986, *Astrophys. J.*, **305**, 805
King, I., 1952, *Astron. J.*, **57**, 253
Koornneef, J., Code, A. D., 1981, *Astrophys. J.*, **247**, 860
Kotani, T., Kawai, N., Aoki, T., et al., 1994, *Publ. Astron. Soc. Japan*, **46**, L147
Kubota, K., Ueda, Y., Fabrika, S., et al., 2010, *Astrophys. J.*, **709**, 1374
Lipunov, V. M., Shakura, N. I., 1982, *Soviet Astron.*, **26**, 386
Margon, B., Ford, H. C., Grandy, S. A., Stone, R. P. S., 1979, *Astrophys. J.*, **233**, L63
Margon, B., 1984, *Annual Review Astron. Astrophys.*, **22**, 507
Marshall, H. L., Canizares, C. R., Schulz, N. S., 2002, *Astrophys. J.*, **564**, 941
Massey, P., Meyer, M. R., 2001. Stellar Masses. In *Encyclopedia of Astron. and Astrophysics*, Nature Publishing Group & Institute of Physics Publishing. Dirac House, Bristol, UK (http://www.astro.caltech.edu/∼george/ay20/eaa-stellarmasses.pdf)
Matthews, T. A., Sandage, A. R., 1963, *Astrophys. J.*, **138**, 30
Mironov, A. V., 2008, *The Basics of Stellar Photometry*, FizMatLit, Moscow, p. 207 (in Russian)
Moro, D., Munari, U., 2000, *Astron. & Astrophys. Suppl. Series*, **147**, 361
Murdin, P., Clark, D. H., Martin, P. G., 1980, *Monthly Not. Roy. Astron. Soc.*, **193**, 135
Nandy, K., Morgan, D. H., Willis, A. J., et al., 1981, *Monthly Not. Roy. Astron. Soc.*, **196**, 955
Newsom, G. H., Collins II, G. W., 1981, *Astron. J.*, **86**, 1250
Newsom, G. H., Collins II, G. W., 1986, *Astron. J.*, **91**, 118
Paragi, Z., Vermeulen, R. C., Fejes, I., et al., 1999, *Astron. & Astrophys.*, **348**, 910
Prevot, M. L., Lequeux, J., Maurice E., et al., 1984, *Astron. & Astrophys.*, **132**, 389
Romney, J. D., Schilizzi, R. T., Fejes, I., Spencer, R.E., 1987, *Astrophys. J.*, **321**, 822
Savage, B. D., Mathys, J. S., 1979, *Annual Review Astron. Astrophys.*, **17**, 73
Schaller, G., Schaerer, D., Meynet, G., Maeder, A., 1992, *Astron. & Astrophys. Suppl. Series*, **96**, 269
Schild, R.E., 1977, *Astrophys. J.*, **82**, 337
Seaton, M. J., 1979, *Monthly Not. Roy. Astron. Soc.*, **187**, 73P
Spencer, R. E., 1984, *Monthly Not. Roy. Astron. Soc.*, **209**, 869
Stephenson, C. B., Sanduleak, N., 1977, *Astrophys. J. Suppl.*, **33**, 459
Straizys, V., 1977, *Multicolor Stellar Photometry*, Mokslas, Vilnius (in Russian)

Straizys, V., Kuriliene, G., 1975, *Bull. Vilnius Obs.*, No. 42, 16
Thorne, K. S., Zytkow, A. N., 1975, *Astrophys. J.*, **199**, L19
Thorne, K. S., Zytkow, A. N., 1977, *Astrophys. J.*, **212**, 832
Vermeulen, R. C., Murdin, P. G., van den Heuvel, E. P. J., et al., 1993a, *Astron. & Astrophys.*, **270**, 204
Vermeulen, R. C., Schilizzi, R. T., Spencer, R. E., et al., 1993b, *Astron. & Astrophys.*, **270**, 177
Wagner, R. M., Newsom, G. H., Foltz, C. B., Byard, P. L., 1981, *Astron. J.*, **86**, 1671
Wagner, R. M., 1986, *Astrophys. J.*, **308**, 152
Yuan, W., Kawai, N., Brinkmann, W., & Matsuoka, M., 1995, *Astron. & Astrophys.*, **297**, 451

Table 1: Mid-eclipse times

JD hel. 24...	σ days	ψ	Source	JD hel. 24...	σ days	ψ	Source
44019.10	0.05	0.156	G	47394.310	0.03	0.955	G
44332.73	0.05	0.088	G	47420.32	0.04	0.114	G
44463.85	0.04	0.896	G	48035.06	0.05	0.903	G
44476.93	0.03	0.975	G	48061.44	0.04	0.066	G
44489.97	0.05	0.058	G	49840.52	0.04	0.030	G
44790.89	0.06	0.910	G	49984.49	0.05	0.914	F
44816.87	0.05	0.073	G	50965.88	0.05		G
45275.10	0.05	0.895	G	50978.61	0.10		G
45928.95	0.04	0.925	G	51763.84	0.05		G
45942.15	0.02	0.006	G	51776.82	0.05		G
45955.18	0.10	0.085	G	52758.00	0.05	0.009	Ir
45968.46	0.10	0.167	G	52770.863	0.05	0.088	Ch
46282.30	0.03	0.102	G	52914.77	0.08	0.975	FG
46583.05	0.10	0.955	G	53582.14	0.02	0.088	G
46596.10	0.04	0.037	G	53595.23	0.04	0.168	G
46936.3047	0.013	0.133	GI	54079.06	0.10	0.150	G:
46936.34	0.04	0.133	G	54380.33	0.02	0.006	K
47093.250	0.03	0.099	G				

G: from the author's data collection; GI: from Ginga X-ray observations; F: S.N. Fabrika;
Ir: T.I. Irsmambetova; Ch: Cherepashchuk et al. (2005); FG: S.N. Fabrika & V.P. Goranskij; K: Kubota et al. (2010).

Table 2: Flux densities of a zero-magnitude A0Vstar in the units of 10^{-9} erg cm^{-2}s^{-1}Å^{-1}

Band	λ_0, Å	$\log_{10}\lambda_0$	Straizys (1977)	Moro & Munari (2000)	This paper
U	3642	3.561	4.22	3.98	4.024
B	4417	3.645	6.40	6.95	6.426
V	5505	3.741	3.75	3.63	3.713
R_C	6469	3.811	–	2.254	2.300
I_C	7886	3.897	–	1.196	1.231

Table 3: Effective wavelengths of light measured for SS 433 in the $UBVR_CI_C$ filters and flux densities of a zero-magnitude A0V type star for this light in the units of 10^{-9} erg cm^{-2}s^{-1}Å^{-1}

Mag	λ_{eff}, Å	$\log_{10}\lambda_{eff}$	f_λ
U	3722	3.571	4.583
B	4623	3.665	5.876
V	5652	3.752	3.455
R_C	6607	3.820	2.153
I_C	7891	3.897	1.228

Table 4: Contribution of emission-line radiation to UBV filters for the eclipse of 2007 October 6 (percents)

Telescope	U^*	B	V	ϕ
Subaru	13.6	15.2	7.6	0.984
BTA	–	18.2	5.1	0.018

* Balmer continuum radiation not taken into account.

Table 5: Theoretical mass–luminosity relation for A stars based on computations in Schaller et al. (1995)

Initial mass	Current mass	$\log M_A$	M_{bol}	$\log L/L_\odot$
4	4.0	0.602	–2.10	2.740
5	5.0	0.699	–3.00	3.100
7	7.0	0.845	–4.35	3.640
9	8.99	0.956	–5.24	3.996
12	11.90	1.076	–6.22	4.338
15	14.70	1.167	–7.02	4.708
20	19.06	1.280	–8.18	5.172
25	23.62	1.373	–8.70	5.380
40	36.06	1.557	–9.50	5.700